Comparison of the performance of some finite element discretizations for large deformation elasticity problems

É. Chamberland[a,*], A. Fortin[a], M. Fortin[a]

[a] *GIREF, Département de mathématiques et de statistique, Pavillon Vachon, 1045 avenue de la médecine, Université Laval, Québec, Canada, G1V 0A6*

Abstract

In this paper, known analytical solutions are used to compare various finite element discretizations for the numerical solution of large deformation problems involving hyperelastic materials. This approach is also known as the method of manufactured solutions (MMS). The performance of these different discretizations is analyzed in terms of convergence in a suitable norm with respect to mesh size, and also in terms of computational cost and memory consumption. Some interesting features of mixed finite element discretizations are presented and discussed. The test cases presented can also serve as non trivial benchmark problems and as a basis for code verification.

Key words: Large deformations, Hyperelastic material, Manufactured solutions, Mixed methods, Convergence order, Code verification.

1. Introduction

The numerical solution of large deformation solid mechanics problems involving non linear materials and complex geometries still represents a challenge to this day. The underlying numerical methodology is complex and irrespectively of the approach used, its implementation is delicate and error prone.

Code verification is a tedious process that cannot be done with a single test. A classical way to make sure that a numerical method is correctly implemented is to solve problems where an analytical solution is known. These problems are however scarce and in many instances oversimplified so that solving them is not sufficient to detect all possible errors. Another strategy is to solve benchmark problems and to make comparisons with the existing literature. This is certainly a valid approach, but these comparisons are often only qualitative and therefore incomplete.

Choosing the most appropriate finite element discretization of the different variables (displacement, pressure) is also a difficult task. This is particularly

*Corresponding author

Email addresses: ericc@giref.ulaval.ca (É. Chamberland), afortin@giref.ulaval.ca (A. Fortin), mfortin@giref.ulaval.ca (M. Fortin)

true for large deformation elasticity problems. A vast choice of possibilities exists ranging from displacement only to various mixed (displacement and pressure) formulations using hexahedra or tetrahedra in three dimensions, triangles or quadrilaterals in two dimensions. Code verification also includes checking the convergence with mesh size of the different variables of the problem using appropriate norms and to compare the results with the existing theory when available.

Code verification, convergence properties and discretization performances can all be established in a very efficient manner by using the method of manufactured solutions (MMS). This concept is very old and can be viewed as just common sense but this idea was set is a systematic code verification frame by Roache [1]. Manufactured solutions are widely used in the CFD community (see Pelletier et al. [2]) but less often in solid mechanics (see Bathe et al. [3]) for example). A manufactured solution is simply an analytical solution to a slightly modified version of the PDE system under consideration. The modification consists generally in the addition of artificial source terms which are easily implemented.

With the elaboration of a manufactured solution, we can pursue three different goals: 1) verify code implementation; 2) check the order of convergence of different discretizations and compare with existing theoretical results; 3) compare the performance of these discretizations with respect to accuracy, computing time and memory consumption.

This paper aims at presenting a systematic way to verify code implementation and to compare discretisation performances for large deformation elasticity problems. Problems having a manufactured solution are solved on a series of progressively refined meshes and the error versus the element size h is plotted. Convergence with mesh size is only one aspect of the performance of a discretisation. Computing times and memory requirements necessary to achieve a given accuracy are other important aspects. To assess this, different plots are presented: error level versus computing time, error level versus number of degrees of freedom, error level versus memory consumption, etc.

The paper is organized as follows. Section 2 provides the equations and variational formulations for both displacement and mixed (displacement and pressure) formulations. Section 3 describes how the method of manufactured solution can be applied for large deformation problems. Section 4 briefly recalls the construction of finite element spaces and the conditions for optimal convergence. Sections 5 and 6 gives the numerical results for the displacement and mixed formulations respectively,

2. Statement of the problem

We will use a total Lagrangian formulation to describe the deformation of an initial domain Ω^0 under the influence of various internal and external forces. The displacement field $\boldsymbol{u}$ links a material point $\boldsymbol{X} = (X_1, X_2, X_3)$ in the reference configuration to its position $\boldsymbol{x}(\boldsymbol{X}, t)$ in the deformed configuration Ω^t following

the relation (see Bonet and Wood [4] and Bathe [5]):

$$(x_1(\boldsymbol{X},t),x_2(\boldsymbol{X},t),x_3(\boldsymbol{X},t)) = (X_1,X_2,X_3) + (u_1(\boldsymbol{X},t),u_2(\boldsymbol{X},t),u_3(\boldsymbol{X},t))$$

The deformation gradient is denoted $\boldsymbol{F}$ with components $F_{ij} = \frac{\partial x_i}{\partial X_j}$ and is related to the displacement gradient $(\boldsymbol{\nabla}_X \boldsymbol{u})_{ij} = \frac{\partial u_i}{\partial X_j}$ by the relation $\boldsymbol{F} = (\boldsymbol{I} + \boldsymbol{\nabla}_X \boldsymbol{u})$. The Cauchy-Green and Green-Lagrange tensors are defined as usual by $\boldsymbol{C} = \boldsymbol{F}^\top \cdot \boldsymbol{F}$ and $\boldsymbol{E} = \frac{1}{2}(\boldsymbol{C} - \boldsymbol{I})$.

On the reference geometry Ω^0, the equilibrium equation can be written as:

$$\left\{ \begin{array}{rcll} -\boldsymbol{\nabla}_X \cdot \boldsymbol{\Pi} & = & \boldsymbol{r}_0 & \text{in } \Omega^0 \\ \boldsymbol{u} & = & \boldsymbol{u}_0 & \text{on } \Gamma_D^0 \\ \boldsymbol{\Pi} \cdot \boldsymbol{N} & = & \boldsymbol{h}_0 & \text{on } \Gamma_N^0 \end{array} \right.$$

In the above system, $\boldsymbol{\Pi}$ is the first Piola-Kirchoff tensor. The boundary Γ^0 of the domain Ω^0 is splitted into two disjoint parts Γ_D^0 and Γ_N^0 where Dirichlet and Neumann boundary conditions are imposed ($\boldsymbol{N}$ is the unit normal vector to Γ_N^0).

The first Piola-Kirchoff tensor is related to the second Piola-Kirchoff tensor $\boldsymbol{S}$ and to the Cauchy stress tensor $\boldsymbol{\sigma}$ by the relation:

$$\boldsymbol{\Pi} = \boldsymbol{F} \cdot \boldsymbol{S} = J \boldsymbol{\sigma} \boldsymbol{F}^{-\top} \quad \text{or} \quad \boldsymbol{\sigma} = \frac{1}{J} \boldsymbol{F} \cdot \boldsymbol{S} \cdot \boldsymbol{F}^\top \tag{1}$$

where $J = \det \boldsymbol{F}$ is the Jacobian of the transformation from Ω^0 to Ω^t.

We will consider here only hyperelastic materials although the methodology is fairly general and can be extended to various materials. In this case, the second Piola-Kirchoff tensor is directly obtained from a potential Ψ by the relation (see [4]):

$$\boldsymbol{S} = \frac{\partial \Psi}{\partial \boldsymbol{E}} = 2 \frac{\partial \Psi}{\partial \boldsymbol{C}}$$

Among the various models that exist, we will consider the Saint-Venant Kirchoff and the Mooney-Rivlin models. The same numerical experiments could be performed for other similar models.

2.1. The Saint-Venant Kirchoff model

The Saint-Venant Kirchoff model is a simple generalization of the elastic model used in small deformation problems. The potential Ψ and the second Piola-Kirchoff tensor can be written as:

$$\Psi = \frac{1}{2}\lambda(\mathrm{tr}\boldsymbol{E})^2 + \mu(\boldsymbol{E}:\boldsymbol{E}), \quad \boldsymbol{S} = \frac{\partial \Psi}{\partial \boldsymbol{E}} = \lambda(\mathrm{tr}\boldsymbol{E})\boldsymbol{I} + 2\mu\boldsymbol{E} \tag{2}$$

where λ and μ are the Lamé coefficients which are related to the Poisson coefficient ν and to Young's modulus E_0 by the relations:

$$\lambda = \frac{E_0 \nu}{(1+\nu)(1-2\nu)} \quad \mu = \frac{E_0}{2(1+\nu)} \tag{3}$$

The variational formulation can be written as:

$$\int_{\Omega^0} (\lambda(\mathrm{tr}\boldsymbol{E})\boldsymbol{I} + 2\mu\boldsymbol{E}) : \left(\boldsymbol{F}^\top \cdot \boldsymbol{\nabla}_X \boldsymbol{w}\right)\, dV = \int_{\Gamma_N^0} \boldsymbol{h}_0 \cdot \boldsymbol{w}\, dA + \int_{\Omega^0} \boldsymbol{r}_0 \cdot \boldsymbol{w}\, dV \quad (4)$$

In the following, this variational formulation will be referred to as a *displacement only* formulation. Eq. (4) is non linear and can be solved for the displacement $\boldsymbol{u}$ using various methods. We will use Newton's method since it converges quadratically.

When the Poisson coefficient ν approaches 0.5, the material gets progressively more incompressible and it is well known that displacement formulations are no longer appropriate and that mixed methods are better suited.

2.2. Mooney-Rivlin material

For incompressible materials, a different formulation is needed and it is more convenient to split the second Piola-Kirchoff tensor into a volumic part and an isochoric part:

$$\boldsymbol{S} = \boldsymbol{S}' - pJ\boldsymbol{C}^{-1} \quad (5)$$

where p is the pressure which is defined by $p = -\kappa(J-1)$. When the bulk modulus κ is large, the material is almost incompressible as it is the case for rubber materials encountered in the tire industry. In this case, one of the most widely used hyperelastic model is the Mooney-Rivlin model which gives (see [4]):

$$\boldsymbol{S}' = 2c_1 I_3^{-1/3}\left(\boldsymbol{I} - \frac{1}{3} I_1 \boldsymbol{C}^{-1}\right) + 2c_2 I_3^{-2/3}\left(I_1 \boldsymbol{I} - \boldsymbol{C} - \frac{2}{3} I_2 \boldsymbol{C}^{-1}\right) \quad (6)$$

where $I_1 = \mathrm{tr}\,\boldsymbol{C}$, $I_2 = \frac{1}{2}(I_1^2 - \boldsymbol{C} : \boldsymbol{C})$ and $I_3 = \det \boldsymbol{C} = J^2$ are the invariants of the tensor $\boldsymbol{C}$. The mixed formulation can now be written as:

$$\begin{cases} \displaystyle\int_{\Omega^0} \boldsymbol{S}' : (\boldsymbol{F}^\top \cdot \boldsymbol{\nabla}_X \boldsymbol{w})\, dV & \displaystyle - \int_{\Omega^0} pJ\boldsymbol{F}^{-\top} : \boldsymbol{\nabla}_X \boldsymbol{w}\, dV & = & \displaystyle\int_{\Gamma_N^0} \boldsymbol{h}_0 \cdot \boldsymbol{w}\, dA + \int_{\Omega^0} \boldsymbol{r}_0 \cdot \boldsymbol{w}\, dV \\ \displaystyle\int_{\Omega^0} (J-1) q\, dV & \displaystyle + \int_{\Omega^0} \frac{1}{\kappa} pq\, dV & = & \displaystyle\int_{\Omega} s_0\, q\, dV \end{cases} \quad (7)$$

In the pressure equation, there is usually no source term ($s_0 = 0$). With manufactured solutions, it is however necessary to account for the possibility of a non-zero source term. This system will also be solved using Newton's method.

3. Elaboration of a manufactured solution

The method of manufactured solution consists in injecting an analytical expression into the PDE under consideration. This generates a right-hand side term in the equation which can be seen as an artificial source term. It is important to carefully chose the manufactured solution so that it exercises all the terms in the variational formulation.

3.1. Step by step construction

The steps for the construction and use of a manufactured solution are essentially the same for both the displacement and the mixed formulations. The description is given for the displacement only formulation. The differences for the mixed formulation are indicated between parenthesis.

1. Choose a manufactured solution for the displacement $\boldsymbol{u}$ (and for the pressure p);
2. Choose material properties λ and μ (or c_1, c_2 and the bulk modulus κ);
3. Compute the deformation gradient $\boldsymbol{F}$;
4. Compute the Green-Lagrange tensor $\boldsymbol{E} = \frac{1}{2}(\boldsymbol{F}^t \cdot \boldsymbol{F} - \boldsymbol{I})$ (or the Cauchy-Green tensor $\boldsymbol{C} = \boldsymbol{F}^\top \cdot \boldsymbol{F}$);
5. Compute the second Piola-Kirchoff tensor $\boldsymbol{S}$ using (2) (or using the decomposition $\boldsymbol{S} = \boldsymbol{S}' - pJ\boldsymbol{C}^{-1}$ with $\boldsymbol{S}'$ given by (6) ;
6. Compute the first Piola-Kirchoff tensor $\boldsymbol{\Pi} = \boldsymbol{F} \cdot \boldsymbol{S}$;
7. Compute the divergence of the first Piola-Kirchoff $\boldsymbol{r}_0 = -\boldsymbol{\nabla}_X \cdot \boldsymbol{\Pi}$ (and the residual term for the pressure: $s_0 = -(\det(\boldsymbol{F}) - 1) - p/\kappa$);
8. Choose a computational domain Ω_0;
9. From the normal $\boldsymbol{N}$ to the reference geometry, compute $\boldsymbol{h}_0 = \boldsymbol{\Pi} \cdot \boldsymbol{N}$ if Neumann boundary conditions are to be imposed;
10. Compute the Cauchy stress tensor $\boldsymbol{\sigma}$ (for comparison purposes only).

Many of the above steps can be performed very efficiently using a symbolic toolkit such as Maple™ or Mathematica®. The choice of an analytical displacement field is *a priori* arbitrary. We have chosen sufficiently regular (smooth) functions so that the expected order of convergence can be observed for all our discretizations.

3.2. Choice of geometry and boundary conditions

When using manufactured solutions, almost any reference geometry Ω^0 can be considered. We have chosen a curved geometry, which is depicted in Fig. 1, that can be seen as a crude approximation of a tire. Curved boundaries introduce an error in the representation of the computational domain. Using curved finite elements may be necessary to obtain a better approximation of the domain and to maintain optimal convergence order.

In our problem, Dirichlet boundary conditions are imposed on the outer and inner curved surfaces of the tire (see Fig. 1) while Neumann boundary conditions are imposed on the flat sides. For Dirichlet conditions, the manufactured solution can be used directly. Neumann conditions are also easily imposed since $\boldsymbol{N}$ is the normal to the undeformed geometry and is therefore easily computed. In the geometry shown of Fig. 1, the unit normal vector on the boundary faces at $Y = 0$ and $Y = 1/4$ is $\boldsymbol{N} = [0, \pm 1, 0]$. From that, the value $\boldsymbol{h}_0 = \boldsymbol{\Pi} \cdot \boldsymbol{N}$ is easily computed (see step 9 in Section 3.1).

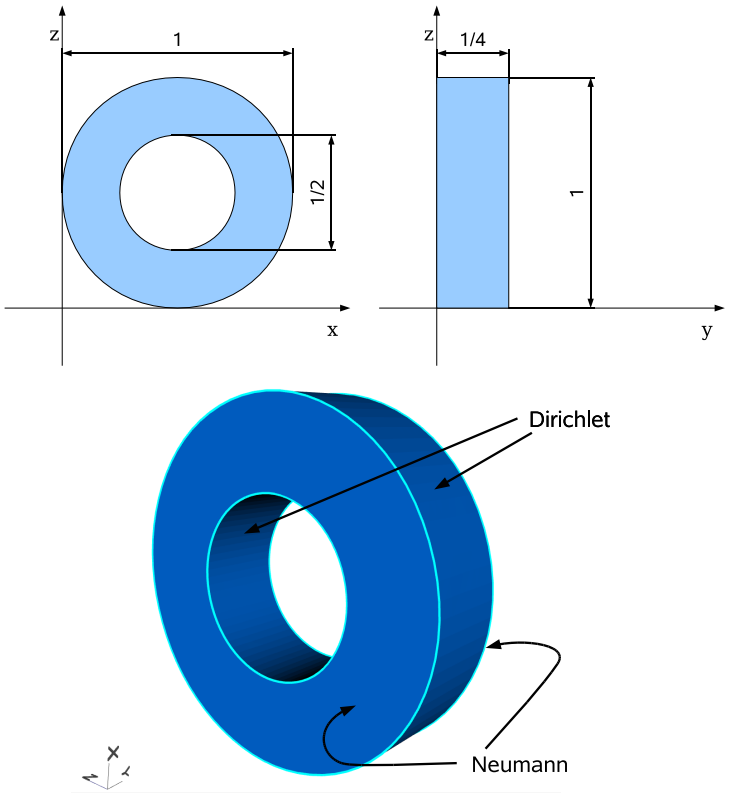

Figure 1: Geometry and boundary conditions of the problem

4. Finite element discretisation spaces

4.1. General considerations

Let us first recall some basic facts concerning the construction of a finite element space. Our notation follows closely that of Arnold et al. [6]. The starting point is a reference domain Ω^0 and a partition (a mesh) of that domain composed of elements K having tetrahedral or hexahedral shape. The next step is the definition of a reference element $\hat{K}$ and a class of invertible mappings T_K from the reference element to the "real" element $K = T_K(\hat{K})$ ($T_K(\xi_1, \xi_2, \xi_3) = (X_1, X_2, X_3)$) where (ξ_1, ξ_2, ξ_3) is a coordinate in the reference element and (X_1, X_2, X_3) its corresponding coordinate in the real element.

Generally speaking, to define a finite element discretization space, it is only necessary to choose a set of polynomials $\hat{V}(\hat{K})$ on the reference element $\hat{K}$. The most natural choices are the space $P_k(\hat{K})$ of polynomials of degree at most k and the space $Q_k(\hat{K})$ of polynomials of degree at most k in each variable. The space $P_k(\hat{K})$ is mostly used on tetrahedral elements while $Q_k(\hat{K})$ is used on hexahedra, but there are exceptions and numerous variations.

This choice of a polynomial basis $\hat{V}(\hat{K})$ automatically defines a space of functions $V_T(K)$ on the real element K by the composition of the functions in $\hat{V}(\hat{K})$ with the mapping T_K^{-1} of the form:

$$V_T(K) = \left\{ v(X_1, X_2, X_3) = \hat{v} \circ T_K^{-1}(X_1, X_2, X_3) \text{ for } \hat{v} \in \hat{V}(\hat{K}) \right\} \tag{8}$$

The simplest situation arises on tetrahedra (triangles in 2D) with affine (linear) mappings T_K. If the space $P_k(\hat{K})$ is chosen, then $V_T(K)$ is naturally the space $P_k(K)$, the space of polynomials of degree k on the element K. When working on hexahedra, the natural mapping is trilinear (Q_1). This allows for general hexahedral meshes with elements having straight edges (quadrilaterals with straight sides in 2D). It may even be necessary to use higher order mappings on domains with curved boundaries for example; $P_2(\hat{K})$ or $Q_2(\hat{K})$ mappings can be used in these cases.

For general approximation theory, it is shown in [6] that in the case of bilinear (or trilinear in 3D) mappings, optimal convergence in L^p-norm can be attained if:

$$V_T(K) \supseteq P_k(K) \tag{9}$$

This is a stronger requirement than the condition $\hat{V}(\hat{K}) \supseteq P_k(\hat{K})$ since it takes into account the mapping T_K. For affine mappings on tetrahedra, it can be easily shown that $\hat{V}(\hat{K}) \supseteq P_k(\hat{K}) \iff V_T(K) \supseteq P_k(K)$ and it is therefore sufficient to require that $\hat{V}(\hat{K})$ contains $P_k(\hat{K})$. This equivalence does not hold in general. In particular, on hexahedra with trilinear mappings, condition (9) will hold only if $\hat{V}(\hat{K}) \supseteq Q_k(\hat{K})$ i.e. the complete set of polynomials of degree k in each variable.

The above result has immediate consequences for second order elliptic problems. If condition (9) is satisfied, setting:

$$V_h = \left\{ v_h \in (H^1(\Omega))^3 \mid v_h|_K \in V_T(K), \forall K \right\} \tag{10}$$

then the finite element discretization error satisfies:

$$\|\boldsymbol{u} - \boldsymbol{u}_h\|_{1,\Omega} \leq C \inf_{v_h \in V_h} \|\boldsymbol{u} - \boldsymbol{v}_h\|_{1,\Omega} \leq h^k \|\boldsymbol{u}\|_{k+1,\Omega} \tag{11}$$

where $h = \max_K h_K$ and h_K is the diameter of the containment sphere of element K. The presence of the H^{k+1}-norm on the right-hand side imposes some regularity on the solution $\boldsymbol{u}$ for this result to hold.

5. Displacement only formulation

Large deformation problems are nonlinear and consequently their numerical analysis is very difficult. We can however rely, at least partially, on the linear case of small deformation problems to conjecture about the behavior of the different discretizations. For (small deformation) displacement formulations, the problem is elliptic and we can apply the results of Section 4. Optimal convergence of order k in H^1-norm should be observed if $V_T(K) \supseteq P_k(K)$.

In our in-house code (see [7]), we can test many different discretizations on hexahedra and tetrahedra. Table 1 (left part) summarises the tetrahedral and hexahedral elements we used in our comparisons. This part of the table defines the different spaces $\hat{V}(\hat{K})$ used in the displacement only formulation. The corresponding finite element spaces are then defined using (10).

For tetrahedral elements, the linear (P_1) and the quadratic (P_2) element were used. The P_2^+ element is a quadratic element enriched with cubic bubble functions at the barycentre of the faces and a quartic bubble function at the barycentre of the element. Finally the third order Hermite (P_3^H) has degrees of freedom for the displacement and its first order partial derivatives at each vertex and for the displacement at the barycentre of the element. For hexahedral elements, the classical 8-noded trilinear Q_1, the complete 27-noded triquadratic Q_2 together with the incomplete (20-noded brick) Q_2^{20} elements were used.

5.1. Meshes, mappings and numerical integration

For our numerical simulations, we have used hexahedral and tetrahedral meshes. Four hexahedral meshes were first constructed by successive refinements of an initial mesh containing 64 elements. This led to meshes with 64, 512, 4096, 32 768 and 262 144 elements (the first and fourth meshes are illustrated in Fig. 2). Note that in the mesh refining process, mid-edge nodes are projected on the curved boundaries of the geometry to maintain a good agreement between the geometry and the surface mesh. Each hexahedral element was then subdivided into 6 tetrahedra producing meshes with 384, 3072, 24 576, 196 608 and 1 572 864 elements.

Isoparametric mappings ($T_K \in \hat{V}(\hat{K})$) from $\hat{K}$ to K were used in all numerical tests. This means that for first order discretizations, tetrahedra and general hexahedra with straight sides were used. For higher order discretizations, P_2, Q_2^{20} and even Q_2 transformations were used producing elements with straight sides inside the domain and elements with curved faces uniquely along the boundary of the domain.

Displacement only		Mixed formulation	
Tetrahedral	Hexahedral	Tetrahedral	Hexahedral
 P_1	 Q_1	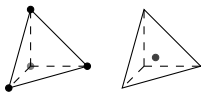 $P_1 - P_0$ †	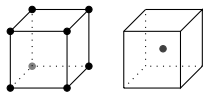 $Q_1 - P_0$ †
 P_2	 Q_2^{20} Incomplete brick	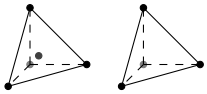 $P_1^+ - P_1$ MINI	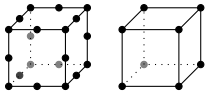 $Q_2^{20} - Q_1$ † Incomplete brick
 P_2^+	 Q_2	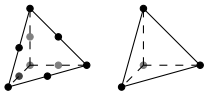 $P_2 - P_1$ Taylor-Hood	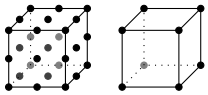 $Q_2 - Q_1$ Taylor-Hood
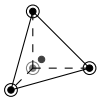 P_3^H Hermite		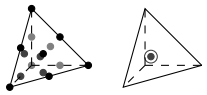 $P_2^+ - P_1^K$ Crouzeix-Raviart	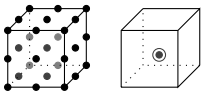 $Q_2 - P_1^K$ Crouzeix-Raviart

Table 1: Finite element discretizations. DOFs are indicated by the symbol •. Symbol ◎ indicates a node the variable and its partial derivatives are unknown. Finally, symbol † indicates elements not satisfying the inf-sup condition.

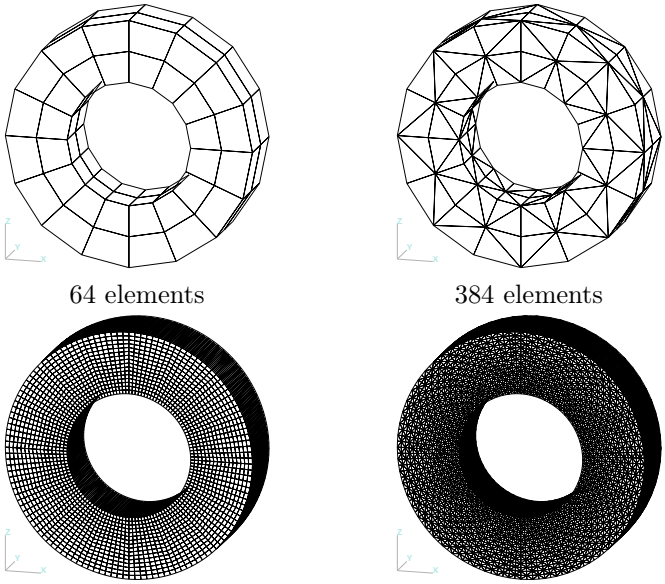

Figure 2: Coarser and finer hexahedral (left) and tetrahedral (right) meshes

Finally, one of the most obvious source of error in finite element computations is the quadrature scheme. In our numerical tests, we chose the lowest possible quadrature formulae independently for each integral term of the variational formulations (4) and (7) in order to minimize the computational cost. Manufactured solutions often lead to complex expressions for $\boldsymbol{r}_0$, s_0 and $\boldsymbol{h}_0$ (produced by Maple$^{\text{TM}}$). To compute these specific terms (and only these ones), a $5 \times 5 \times 5$ (125 points) Gauss-Legendre integration scheme on hexahedra and a 53 points scheme on tetrahedra (see [8]) were used. For Neumann boundary conditions, we used a 5×5 Gauss-Legendre scheme for the quadrangles and a 37 points scheme for the triangles (see [9]). Classical integration formulae were used for all the other terms in the variational formulation.

5.2. Convergence with mesh size

To achieve our second and third goals, which are to verify the convergence order of the discretizations and to assess their respective performance, we will use a manufactured function of a degree higher than any of the proposed discretizations. For instance, let:

$$\boldsymbol{u} = \left[{X_1}^4 + \frac{2X_2X_3}{5}, {X_2}^4 + \frac{2X_1X_3}{5}, \frac{{X_3}^4}{10} - \frac{2X_1X_2X_3}{5} \right]$$

with material properties $\nu = 0.3$ and $E_0 = 1$. Following the steps for the construction of a manufactured solution, the source terms $\boldsymbol{r}_0$, s_0 and $\boldsymbol{h}_0$ are

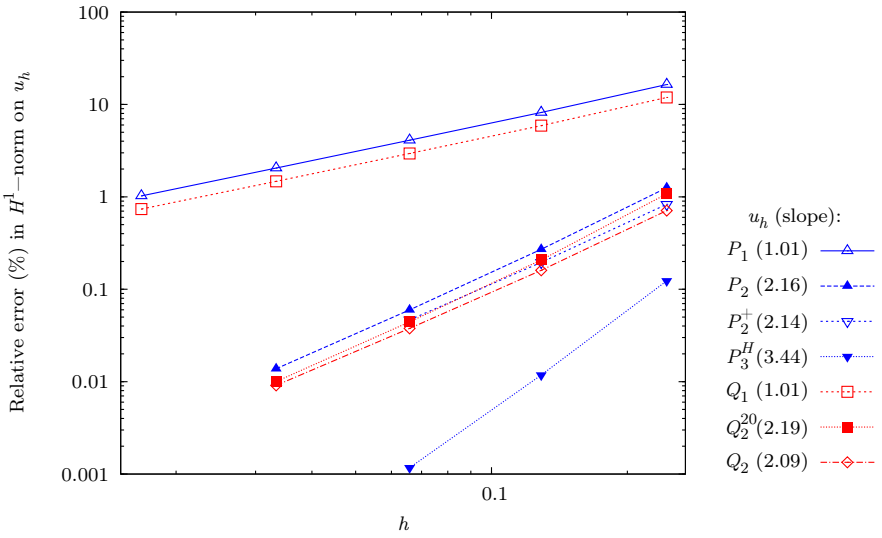

Figure 3: Relative error ($||u-u_h||_{1,\Omega_h}/||u||_{1,\Omega_h}$) as a function of the maximum element length (h)

computed and put into a compatible input file for our in-house code. Our Maple$^{\text{TM}}$worksheet is available for download (see [10]).

We first compare the results for the H^1-norm of the error on the displacement. The asymptotic slope on a log-log scale of the relative error norm versus the mesh size (h) is computed for each given discretization. Fig. 3 gives an overview that facilitates the identification of the trends in the behavior of the error norm for the chosen discretizations.

We can observe that the calculated slopes are very close to those expected from theory. We can easily distinguish between first, second and third order elements. Discretizations of the same order yield similar slopes and comparable error levels. Second order hexahedral elements are just slightly more accurate than their tetrahedral counterparts. This is no surprise since their polynomial basis is richer ($Q_2 \supset P_2$) and it is expected that they give more accurate approximations for a given manufactured solution. The norm of the error on the finest mesh is 0.009% for the Q_2 element and 0.013% for the P_2 element. The difference is thus very small.

The amplitude of the error level is however surprisingly high for first order elements and in particular for the very popular Q_1 element. The error obtained on the finest mesh (with 836 352 DOFs) is about the same as the one obtained with the coarsest mesh using the incomplete quadratic discretization (with 1440 DOFs) at around 0.8%. High order elements are thus more accurate even on much coarser meshes and it is therefore clearly unfair to compare the different discretizations on the same mesh. Note however that these conclusions can be

drawn since we have chosen a regular manufactured solution. Higher order discretisations require higher regularity for optimal convergence. The conclusions may be different for an insufficiently regular manufactured solution.

A few words are necessary to weigh the very good performance of the Q_2^{20} element. This element is a very simple example where $\hat{V}(\hat{K}) \supseteq P_2(\hat{K})$ while $V_T(K) \not\supseteq P_2(K)$. From the discussion of Section 4 and as was observed in Lee and Bathe [11] and later in [6], it is possible to obtain second order convergence only on meshes composed of affine elements. On general meshes, the Q_2^{20} element is unable to reproduce a quadratic manufactured solution and convergence can degenerate to first order, but the accuracy is still better than the one obtained for the Q_1 element. Second order convergence on general meshes can be achieved for the complete Q_2 element only.

Quadratic convergence is indeed observed for the Q_2^{20} element even though the meshes are made of general hexahedra. With the geometry at hand however, the elements are very close to parallelepipeds. When refining a general mesh in the usual manner, by simply dividing the edges, the elements get closer and closer to parallelepipeds and optimal convergence may reappear. This is the case with the meshes of Fig. 2.

To observe suboptimal convergence, each node of the initial meshes were randomly perturbed in such a way that the elements on all meshes remain with non parallel faces. Suboptimal convergence ($m = 1.73$) for the Q_2^{20} element can be observed in Fig. 4. Further decreasing h would probably lead to a unit slope as was observed in [6, 11] for two-dimensional problems.

5.3. Performance comparison

Another dimension is added to the evaluation of the performance of the discretizations by also comparing the computational times and the memory requirements for each discretization on different meshes. We thus compute the L^2-norm of the error on the Cauchy stress tensor ($\|\boldsymbol{\sigma} - \boldsymbol{\sigma}_h\|_{0,\Omega}$). Computing the L^2-norm of the error on this important variable serves as a basis for the comparisons.

This relative error norm on $\boldsymbol{\sigma}$ is thus plotted in Fig. 5 as a function of the number of DOFs, the total CPU time an the memory necessary to make the computation. The measure includes all the CPU time from the reading to the writing of results and it is largely dominated by the matrix factorization. Using these figures, we can more easily decide which discretization is best for a given computational time. For this regular manufactured solution, the conclusions that can be drawn are the following: *For a given computational cost or a given number of DOFs or a given memory consumption, higher order elements are more accurate.* Whether from the perspective of minimizing the error norm for a given computational cost or minimizing the computational cost for a given error norm, higher order elements are more cost effective. The elements rank approximately as: P_3^H, Q_2^{20}, Q_2, P_2, P_2^+, Q_1 and then the P_1 in terms of computational efficiency. We can also make a couple of important remarks:

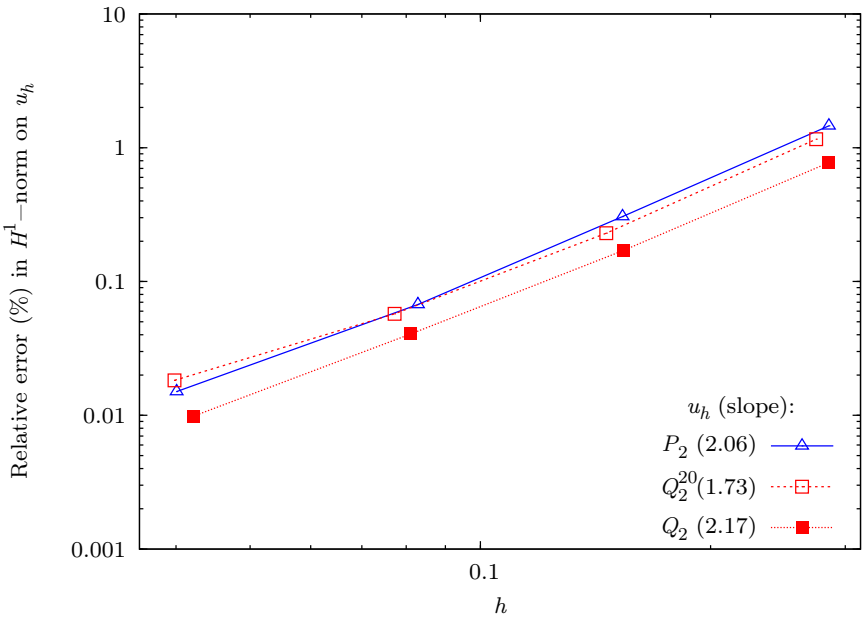

Figure 4: Relative error ($||u-u_h||_{1,\Omega_h}/||u||_{1,\Omega_h}$) as a function of the maximum element length (h) for randomly perturbed meshes showing the non-optimal convergence for the Q_2^{20} element

- Q_1 and P_1 solutions are not at all cost effective when the accuracy of the solution is taken into account. For a given computational cost in terms of CPU time and memory, it is still preferable to use higher order elements on a much coarser mesh because the error level is lower.
- The Hermite element is probably not a judicious choice since the imposition of Dirichlet boundary conditions is more difficult due to the presence of DOFs associated to the first order partial derivatives of the displacement. However, similar results in terms of precision and efficiency could probably be obtained with a Lagrange cubic element (P_3).
- A good compromise is therefore a second order element such as the P_2 or the (complete) Q_2 elements.

5.4. Curved boundaries and subparametric elements

We close this section with a final remark concerning the presence of curved boundaries and the importance of using isoparametric mappings. For second order elements, it is necessary to use isoparametric mappings T_K to maintain optimal convergence order. Strang and Berger [12] have shown that when using the subparametric P_2 element (with P_1 mappings), $O(h^{3/2})$ convergence rate is observed in H^1-seminorm instead of the optimal second order rate. We have also observed this suboptimal convergence on one of our manufactured solution.

6. Mixed displacement-pressure formulation

Although the analysis is more complicated for mixed formulations, it is now classical at least in the small deformation case. As we shall see, the conclusions for mixed (displacement-pressure) formulation are similar to those drawn for the displacement only formulation. There exists a large number of mixed elements i.e. pairs of discretizations for the displacement and the pressure that can be used to solve large deformation problems. Some of them satisfy the inf-sup condition and others do not. We have restricted our study to those most often found in the literature. It is outside the scope of this paper to demonstrate which pair satisfies this condition and we refer to Brezzi and Fortin [13] and to Boffi et al. [14] for a complete discussion.

6.1. Theoritical considerations

Two finite element spaces must be chosen. The displacement finite element space can be written as before:

$$V_h = \left\{ v_h \in (H^1(\Omega))^3 | \forall K, v_h|_K \in V_T(K), \forall K \right\}$$

while for the pressure, we must distinct two possible cases. For continuous pressure, we define:

$$Q_h = \left\{ q_h \in L^2(\Omega) | \forall K, q_h|_K \in Q_T(K), \forall K \right\}$$

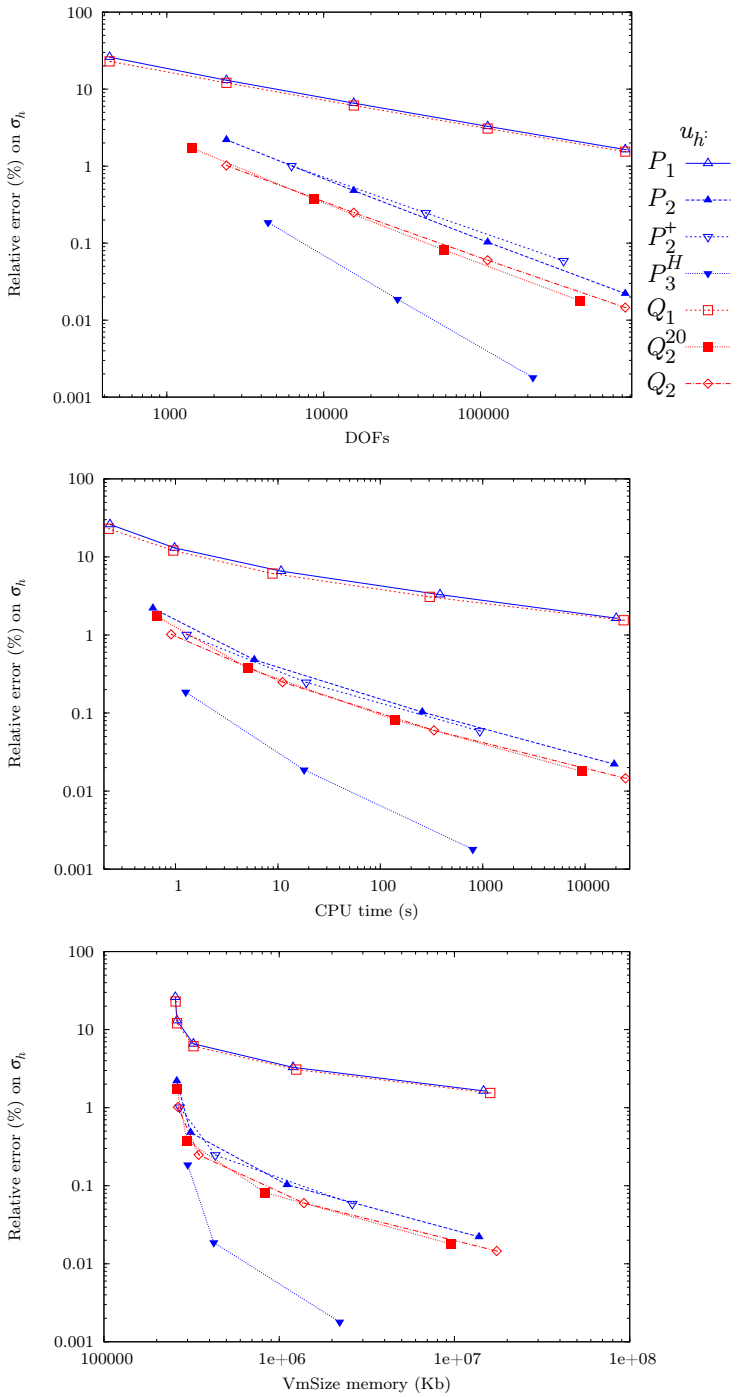

Figure 5: Displacement formulation: relative error on $\boldsymbol{\sigma}$ (L^2-norm) as a function of the number of DOFs, the CPU time and memory.

where $Q_T(K)$ is usually defined as was $V_T(K)$. As discussed in [15] for the Stokes problem, this is however not necessarily the best choice. For discontinuous pressure discretization, there exists two choices. For example, for a so-called linear discontinuous pressure, we can choose $\hat{Q}(\hat{K}) = P_1(\hat{K})$ and:

$$Q_h = P_1^{\hat{K}} = \left\{ q_h \in L^2(\Omega) | \forall K, q_h|_K = \hat{q} \circ T_K^{-1}(x, y, z) \text{ for } \hat{q} \in P_1(\hat{K}) \right\}$$

and therefore the functions in $P_1^{\hat{K}}$ are linear on the reference element $\hat{K}$ but not necessarily linear on the real element K, depending on T_K. This is probably the most common frequently used definition. We can also use the following definition:

$$Q_h = P_1^K = \left\{ q_h \in L^2(\Omega) \middle| q_h|_K = a^K + \sum_{i=1}^{3} g_i^K (X_i - X_i^K) \ , \ \ \forall K \right\}$$

where (X_1^K, X_2^K, X_3^K) is the barycenter of the element K. With this choice, the degrees of freedom a_K and (g_1^K, g_2^K, g_3^K) are respectively the value of the pressure and its gradient at (X_1^K, X_2^K, X_3^K). The functions in P_1^K are now linear on K. On tetrahedral meshes with linear mappings T_K, the two definitions are equivalent. On general hexahedral meshes, P_1^K contains $P_1(K)$ while $P_1^{\hat{K}}$ does not. This leads to suboptimal convergence when $P_1^{\hat{K}}$ is used for discontinuous pressure. We have observed results (not presented) similar to those in [15] for large deformation problems in three dimensions.

A compatibility condition between the displacement and pressure discretizations must be respected known as the inf-sup condition, which is described in details in [13, 14]. This condition can be written as:

$$\inf_{q_h \in Q_h} \sup_{v_h \in V_h} \frac{\int_\Omega q_h \nabla \cdot \boldsymbol{v}_h}{||\boldsymbol{v}_h||_{1,\Omega} \ ||q_h||_{0,\Omega}} \geq \alpha_h > \alpha > 0 \tag{12}$$

The constant α_h always exists, but may depend on h or be equal to zero. In order to satisfy the inf-sup condition, it must be bounded from below by a positive constant α which does not depend on h. Note that to different pairs of discretizations satisfying the inf-sup condition (12), correspond different values of α. When the inf-sup condition is satisfied, then the finite element discretization error satisfies (see [13] pages 56-57):

$$\begin{aligned} \|\boldsymbol{u} - \boldsymbol{u}_h\|_{1,\Omega} &\leq c_1(\alpha) \inf_{v_h \in V_h} \|\boldsymbol{u} - \boldsymbol{v}_h\|_{1,\Omega} + c_2 \inf_{q_h \in Q_h} \|p - q_h\|_{0,\Omega} \\ \|p - p_h\|_{0,\Omega} &\leq c_3(\alpha) \inf_{q_h \in Q_h} \|p - q_h\|_{0,\Omega} + c_4(\alpha) \|\boldsymbol{u} - \boldsymbol{u}_h\|_{1,\Omega} \end{aligned} \tag{13}$$

The constants $c_i(\alpha), i = 1, 3, 4$ are $O(\alpha^{-1})$ functions (but not c_2). Hence, the error estimate on the pressure is $O(\alpha^{-2})$. For a fixed space Q_h, enriching V_h will increase α and in the same time the accuracy of the solution. Conversely, for a fixed space V_h, enriching Q_h will decrease α and this may have dramatic

consequences on the accuracy of the pressure and, ultimately, of the displacement.

The order of convergence of the discretization will depend on both spaces V_h and Q_h for the displacement and the pressure. Succinctly, if $V_T(K) \supseteq P_k(K)$ (displacement) and $Q_T(K) \supseteq P_{k-1}(K)$ for the pressure, then:

$$\|\boldsymbol{u} - \boldsymbol{u}_h\|_{1,\Omega} + \|p - p_h\|_{0,\Omega} \leq Ch^k \left(\|\boldsymbol{u}\|_{1,\Omega} + \|p\|_{0,\Omega}\right) \tag{14}$$

and this holds for general meshes.

Note however that the above (linear) analysis does not give the complete picture. As described in Pantuso and Bathe [16, 17] in a displacement-pressure-enhanced strain formulation and Auricchio et al. [18] for a displacement-pressure formulation, elements satisfying the inf-sup condition may present numerical instabilities in the large deformation case. It can be shown that these instabilities are explained by a failure in the ellipticity condition. The importance of the ellipticity condition is also discussed in Brezzi and Bathe [19]. One such example is the MINI element (see section 6.4.1) which may be unstable in some conditions even though it satisfies the inf-sup condition.

6.2. Choice of discretizations

The different mixed discretizations (the spaces $\hat{V}(\hat{K})$ and $\hat{Q}(\hat{K})$) tested in the following numerical tests are presented in Table 1. The simplest choice is the $P_1 - P_0$ (linear for the displacement and piecewise constant for the pressure) which does not verify the inf-sup condition. This is a poor choice probably at the origin of the myth that tetrahedral elements are not suited for incompressible solid mechanic problems.

The most popular choice is the $Q_1 - P_0$ element for which the displacement is trilinear while the pressure is piecewise constant.It does not satisfy the inf-sup condition either, but is nevertheless frequently used probably due to its simplicity. Another advantage is that the pressure can be eliminated by penalization. For these reasons, it is generally recognized as an effective and low cost element.

The simplest element satisfying the inf-sup condition is the MINI element introduced by Arnold et al. [20] and also denoted $P_1^+ - P_1$. It is mainly used in CFD applications. Since in this case $V_h \supseteq P_1$ and $Q_h \supseteq P_1$, Eq. (14) makes it a first order ($O(h)$) element.

Second order elements are represented by the Taylor-Hood [21] element $P_2 - P_1$ and by the Crouzeix-Raviart [22] elements: $P_2^+ - P_1^K$ on tetrahedra, and $Q_2 - P_1^K$ on hexahedra. We have also tested the incomplete quadratic $Q_2^{20} - Q_1$ which, to the authors knowledge, does not satisfy the inf-sup condition.

6.3. Convergence with mesh size

For this test, we use the Mooney-Rivlin model with $k = 10\,000$, $c_1 = 1$ and $c_2 = 2$. The manufactured solution is:

$$\boldsymbol{u} = \frac{1}{200}\left[X_1^3 X_2^4 X_3^4, X_1^3 X_2^3 X_3^4, X_1^3 X_2^3 X_3^3\right] \quad \text{and} \quad p = \frac{X_1^3}{200} + \frac{X_2^4}{100} + \frac{X_3^2}{250}$$

The convergence slopes obtained by each discretization are shown in Fig. 6 for the displacement and the pressure. In all cases, the slopes of the curves are what is expected from theory, except for the $P_1^+ - P_1$ element for which the slope is slightly higher than 1. This slope should however tend towards 1 if the meshes are further refined.

The $P_1 - P_0$ element gives extremely inaccurate results and should never be used under any circumstances. The $Q_1 - P_0$ element performs better with a 2% error on the displacement and 0.8% error on the pressure on the finest mesh (262 144 elements!), but this is still very disappointing. The MINI ($P_1^+ - P_1$) element has a similar accuracy and is therefore also disappointing. All second order elements are clearly more accurate as expected. The error on the coarsest mesh for both the displacement and pressure is comparable to the error on the finest mesh for linear elements. The performances of the different hexahedral elements are indistinguishable but, as in the displacement formulation, they are more accurate than their tetrahedral counterparts.

6.4. Performance comparison

Here again, the accuracy on the Cauchy stress tensor is a good indicator of the performance of a mixed element since its computation involves both the displacement and the pressure (see Eqs. (1) and (5)). The results for all elements are illustrated in Fig. 7.

6.4.1. The $Q_1 - P_0$ and the MINI elements

Although the $Q_1 - P_0$ does not satisfy the inf-sup condition and, on the contrary, the MINI ($P_1^+ - P_1$) element does satisfy this condition, these two elements present comparable performances.

For the $Q_1 - P_0$ element, it is well known that spurious pressures taking the form of a checkerboard may be present in certain situations. We had a hard time trying to find cases where a checkerboard appeared with a manufactured solution. It is a lot easier to illustrate this catastrophic situation by simply compressing a cubic domain ($k = 1000$) by imposing Dirichlet boundary conditions on the two opposite faces (not illustrated).

The MINI element is hardly used in solids analysis, because the stress predictions are obviously too poor for the effort involved. The velocity bubble can be statically condensed out but this is not possible for the pressure since it is continuous. It only has found some use in fluids analysis and was considered here only as an example of a stable low order element. Although we have observed linear convergence for this element, it has major drawbacks. On general meshes, obtained by dividing hexahedra into 6 tetrahedra (equivalent to the division of a quadrangle into two triangles in two dimensions), the pressure is polluted by oscillations (not illustrated) whose amplitude tends towards 0 as the mesh is refined.

6.4.2. Second order elements

From Fig. 7, the best choice is the $Q_2^{20} - Q_1$ element. This element suffers however from the same weakness on general hehahedral meshes as the Q_2^{20} in the

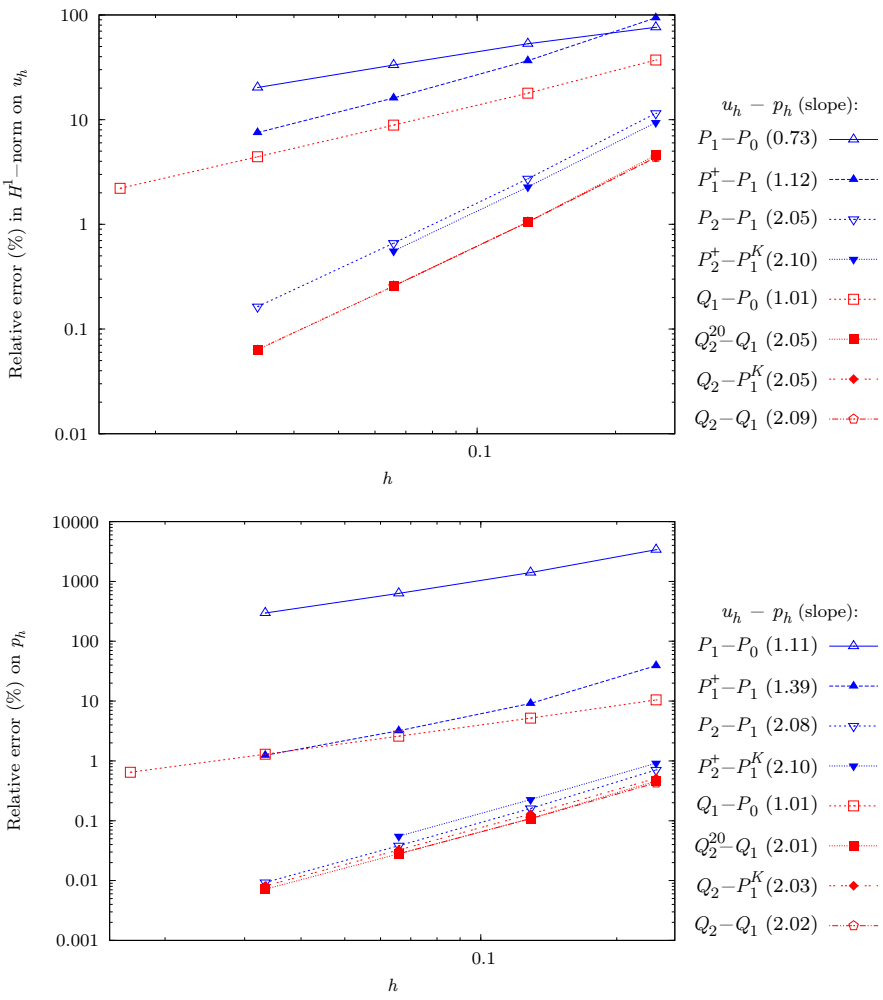

Figure 6: Relative error on displacement (H^1-norm) and pressure (L^2-norm) as a function of mesh size.

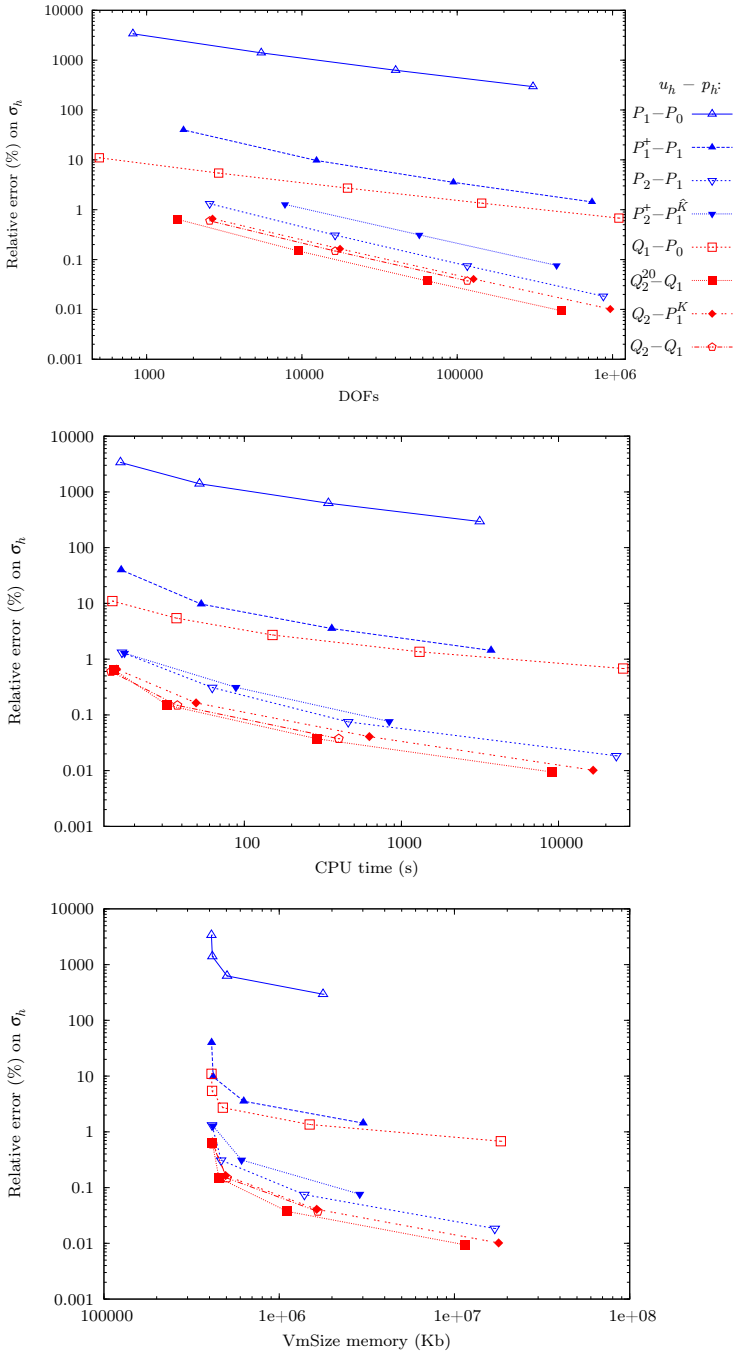

Figure 7: Mixed formulation: relative error on $\sigma(L^2$-norm) as a function of the number of DOFs, the CPU time and memory.

displacement formulation. The explanation is exactly the same and we cannot recommand its use in general.

All other second order elements presents interesting performances. Both Crouzeix-Raviart elements ($P_2^+ - P_1^K$ and $Q_2 - P_1^K$) are slightly disadvantaged by their large number of DOFs but they still perform rather well. From the overall results of Fig. 7, we can advocate the use of these elements for nearly incompressible large deformation problems. They perform extremely well on all aspects of our study: accuracy, CPU time, memory space, etc.

6.4.3. Using discontinuous pressure

Elements with discontinuous pressure are very advantageous since it can be statically condensed out. This makes them extremely efficient. We confirm the results of [14] that using the $Q_2 - P_1^K$ (linear pressure on K) gives better results than with the $Q_2 - P_1^{\hat{K}}$ (linear pressure on $\hat{K}$). The slopes of the convergence curves on the pressure (not illustrated) were 2.61 and 1.52 respectively.

6.4.4. Enriching the pressure discretization space

Comparing the accuracy of the $P_2 - P_1$ and $P_2^+ - P_1^K$ elements, we found, on some manufactured solutions, that the level of error on the pressure was higher for the latter (and richer) element (see Fig. 8). The explanation comes from the observation already made that a richer approximation for the pressure leads to a smaller value of α in the inf-sup condition (12). We have also observed that the discretization error for the pressure is proportional to $1/\alpha^2$. In order to confirm that this explanation is valid, we have compared the errors obtained with the $P_2^+ - P_1^K$ and the $P_2^+ - P_1$ elements. The only difference between these two elements is the pressure space which is larger for the P_1^K. Fig. 8 shows that the corresponding error is also larger.

6.4.5. The H^1-seminorm of p_h as an oscillation indicator

During the course of our numerical experiments, it appeared that computing the H^1-seminorm of the error on the pressure was a convenient measure of oscillating pressures. This is easy to compute for continuous pressure approximations but it cannot be done directly if the pressure is discontinuous. In this last case, the pressure can be projected in L^2-norm onto a richer continuous approximation space like Q_2 or P_2. To observe oscillations in the pressure, and in particular for the $Q_1 - P_0$ element, it is essential to use a manufactured solution with $\det \boldsymbol{F}$ slightly different from 1, a bulk modulus k of at least 1000 and meshes with randomly perturbed nodes. Computations with these parameters were done, the seminorm has been computed and the results are presented in Fig. 9.

On this graph, we can see that all elements that may present problems display non-optimal convergence. MINI and the $Q_1 - P_0$ do not converge and this is also the case for the $Q_2 - P_1^{\hat{K}}$ element. The $Q_2^{20} - Q_1$ converge but with a lower rate than the other quadratic elements.

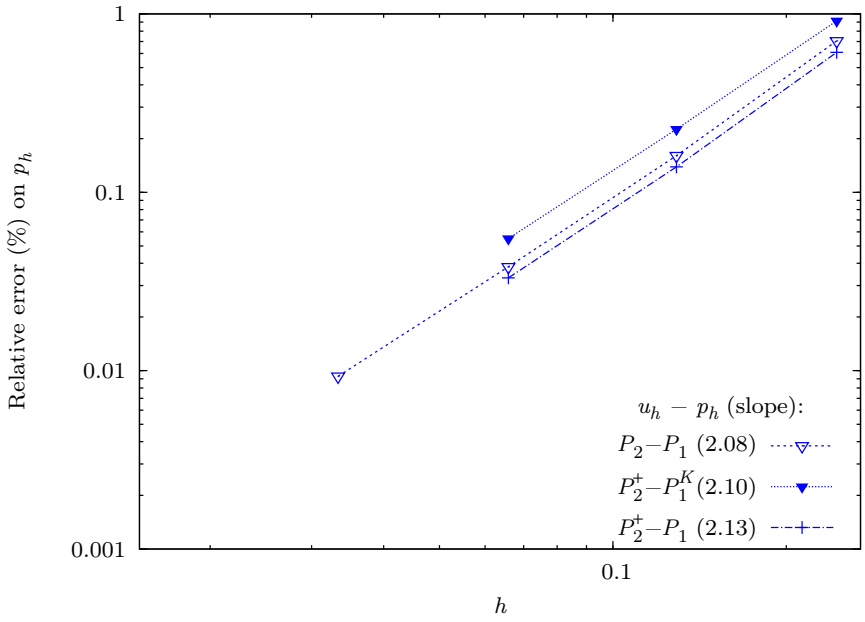

Figure 8: Relative error ($||p-p_h||_{0,\Omega_h}/||p||_{0,\Omega_h}$) as a function of the maximum element length (h) showing larger error with the $P_2^+ - P_1^K$ element compared to the $P_2^+ - P_1$ element

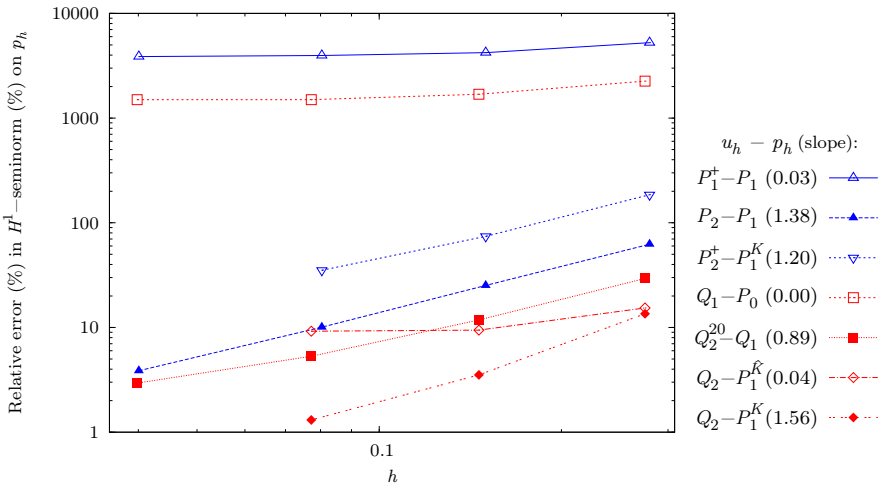

Figure 9: Relative error ($|p-p_h|_{1,\Omega_h}/|p|_{1,\Omega_h}$) as a function of the maximum element length (h)

Even though the theory does not say anything about the convergence of the pressure in this norm, we can say that computing the H^1-seminorm of the pressure underlines the differences in the behavior of the different discretizations. It may thus be used as a simple indicator to test mixed finite element discretizations, and in particular to detect checkerboards effects or more generally, oscillating pressures.

7. Conclusions

The method of manufactured solutions offers a systematic strategy to verify a finite element software and to establish experimentally the convergence order of a given discretization. In this paper, it was also used to compare various discretizations among them. Methodic use of the method of manufactured solutions makes it possible to detect the weaknesses of the different discretizations and to clearly establish which elements are suitable to a particular finite element formulation.

In the presented test cases, first order elements such as P_1 and the Q_1 elements in the displacement only formulation, or the MINI, the $P_1 - P_0$ and the $Q_1 - P_0$ elements in displacement-pressure formulation were shown to give large error norms even on the finest meshes. The MINI element, in particular, performs rather poorly. Satisfying the inf-sup condition is therefore not a sufficient condition to decide on the usefulness of an element.

We have demonstrated experimentally that incomplete polynomial spaces on non affine meshes may lead to suboptimal convergence. Linear (on the real element) discontinuous pressure P_1^K performed better that the linear (on the reference element) $P_1^{\hat{K}}$.

We have shown that second order elements present many advantages in terms of accuracy and computational efficiency. These conclusions were already obtained in Bathe [5, 23]. Rigorous comparisons of various discretizations in terms of DOFs, memory consumption or CPU time led to the conclusion that second order elements are best and in particular, the P_2 and Q_2 elements for displacement only formulation and the $P_2 - P_1$ or $Q_2 - P_1^K$ mixed elements are very good choices in general. In all aspects, second order elements perform better than first order ones, at least for regular solutions.

We would like to emphasize that when using general (non affine) meshes, the performances of tetrahedral and hexahedral elements of the same order are similar. It shows that tetrahedra are also well suited for large deformation problems. It is now possible to find good hexahedral meshers, though it is fair to say that meshing a complex three-dimensional geometry is still easier to do with a tetrahedral mesher. Most of the time, mesh adaptation is based on tetrahedra even though it is possible to locally adapt a hexahedral mesh. It is however very difficult to introduce anisotropic adaptation using hexahedra. Anisotropic meshes, which include elements with very large aspect ratio, would help to improve the accuracy of numerical solutions, while reducing the computational burden and this leads us to favor tetrahedral discretizations.

We are now extending the method of manufactured solution to frictional contact problems. Various discretizations of the displacement, pressure and contact forces can be compared. Preliminary results on unilateral contact are promising showing the usefulness of this approach (see Chamberland et al. [24]).

Acknowledgments

The authors wish to acknowledge the financial support of the Natural Sciences and Engineering Research Council of Canada (NSERC)

References

[1] P. J. Roache. Code verification by the method of manufactured solutions. *Journal of Fluids Engineering*, 124(1):4–10, 2002. Available from: http://link.aip.org/link/?JFG/124/4/1, doi:10.1115/1.1436090.

[2] D. Pelletier, É. Turgeon, D. Lacasse, and J. Borggaard. Adaptivity, Sensivity and Uncertainty: Towards Standards in CFD. In *39th AIAA Aerospace Sciences Meeting and Exibit*, 2001.

[3] K.J. Bathe, M. Bucalem, and F. Brezzi. Displacement and stress convergence of our MITC plate bending elements. *J. Eng. computations*, 7(4):291–302, 1990. Available from: http://dx.doi.org/10.1108/eb023816, doi:10.1108/eb023816.

[4] J. Bonet and D. R. Wood. *Nonlinear continuum mechanics for finite element analysis*. Cambridge University Press, Cambridge, 1997. Available from: http://www.cambridge.org/us/catalogue/catalogue.asp?isbn=0521838703.

[5] K. J. Bathe. *Finite Element Procedures*. Prentice Hall, 1996. Available from: http://www.pearsonhighered.com/educator/academic/product/0,3110,0133014584,00.html.

[6] D. N. Arnold, D. Boffi, and R.S. Falk. Approximation by quadrilateral finite element. *Math. Comp.*, 71(239):909–922, 2002. Available from: http://dx.doi.org/10.1090/S0025-5718-02-01439-4, doi:10.1090/S0025-5718-02-01439-4.

[7] GIREF. http://www.giref.ulaval.ca/projets/. Available from: http://www.giref.ulaval.ca/projets/.

[8] M. Beckers and A. Haegemans. The construction of cubature formulae for the tetrahedron. *Report TW 128, Dept. of Computer Science, K.U. Leuven*, 1990.

[9] D. A. Dunavant. High degree efficient symmetrical Gaussian quadrature rules for the triangle. *Int. J. Numer. Methods Engrg.*, 21(6):1129–1148, 1985. Available from: http://dx.doi.org/10.1002/nme.1620210612, doi:10.1002/nme.1620210612.

[10] É. Chamberland. Feuille Maple pour la méthode des solutions manufacturées en grandes déformations http://www.giref.ulaval.ca/~ericc/mms. Available from: http://www.giref.ulaval.ca/~ericc/mms.

[11] N.-S. Lee and K. J. Bathe. Effects of element distortions on the performance of isoparametric elements. *International Journal for Numerical Methods in Engineering*, 36(20):3553–3576, 1993. Available from: http://dx.doi.org/10.1002/nme.1620362009, doi:10.1002/nme.1620362009.

[12] G. Strang and A. E. Berger. The change in solution due to change in domain. In *Proceedings of the Symposium in Pure Mathematics, Partial Differential Equations*, volume 23, pages 199–205. AMS Bookstore, 1973. Available from: http://www.ams.org/bookstore?fn=20&arg1=pspumseries&item=PSPUM-23.

[13] F. Brezzi and M. Fortin. *Mixed and Hybrid Finite Element Methods*, volume 15 of *Springer series in computational mathematics*. Springer-Verlag, New York, 1991. Available from: http://portal.acm.org/citation.cfm?id=108342&dl=GUIDE&coll=GUIDE&CFID=30898868&CFTOKEN=25543202.

[14] D. Boffi, F. Brezzi, L. F. Demkowicz, R. G. Durán, Falk R. S., and M. Fortin. *Mixed finite elements, compatibilty conditions, and applications*, volume 1939 of *Lecture notes in mathematics*. Springer, 2008. Available from: http://dx.doi.org/10.1007/978-3-540-78319-0, doi:10.1007/978-3-540-78319-0.

[15] L. Gastaldi and D. Boffi. On the quadrilateral Q2-P1 element for the Stokes problem. *International Journal for Numerical Methods in Fluids*, 39(11):1001–1011, 2002. Available from: http://dx.doi.org/10.1002/fld.358, doi:10.1002/fld.358.

[16] D. Pantuso and K. J. Bathe. A four-node quadrilateral mixed interpolated element for solids and fluids. *Mathematical models and methods in applied sciences*, 5(8):113–1128, 1995. Available from: http://dx.doi.org/10.1142/S0218202595000589, doi:10.1142/S0218202595000589.

[17] D. Pantuso and K. J. Bathe. On the stability of mixed finite elements in large strain analysis of incompressible solids. *Finite Elements in Analysis and Design*, 28(2):83–104, 1997. Available from: http://www.sciencedirect.com/science/article/B6V36-3SYPT87-1/2/fc1aba87f350a00376679c63bcb91ca7, doi:10.1016/S0168-874X(97)81953-1.

[18] F. Auricchio, L. Beirão da Veiga, C. Lovadina, and A. Reali. A stability study of some mixed finite elements for large deformation elasticity problems. *Computer Methods in Applied Mechanics and Engineering*, 194(9-11):1075 – 1092, 2005. Available from: http://www.sciencedirect.com/science/article/B6V29-4D5JX5V-1/2/91f2ee48546f3ac70ffbd2ce2dc9d241, doi:DOI: 10.1016/j.cma.2004.06.014.

[19] F. Brezzi and K.J. Bathe. A discourse on the stability conditions for mixed finite element formulations. *Computer Methods in Applied Mechanics and Engineering*, 82(1-3):27 – 57, 1990. Proceedings of the Workshop on Reliability in Computational Mechanics. Available from: http://www.sciencedirect.com/science/article/B6V29-47SVFNH-4/2/900037c542f87f729c9db76e02392915, doi:10.1016/0045-7825(90)90157-H.

[20] D. N. Arnold, F. Brezzi, and M. Fortin. A stable finite element for the Stokes equations. *Calcolo*, 21:337–344, 1984. Available from: http://www.springerlink.com/content/a54722r712511871, doi:10.1007/BF02576171.

[21] C. Taylor and P. Hood. Numerical solution of the Navier-Stokes equations using the finite element technique. *Computers and Fluids*, 1(1):73–100, 1973. Available from: http://www.sciencedirect.com/science/article/B6V26-480TTGH-3T/2/7adfcd863eabca005cfbb31322b4c4c6, doi:10.1016/0045-7930(73)90027-3.

[22] M. Crouzeix and P. A. Raviart. Conforming and non-conforming finite element methods for solving the stationary Stokes equations. *RAIRO Anal. Numer*, 7:33–76, 1973.

[23] K. J. Bathe. The finite element method. In B. Wah, editor, *Encyclopedia of Computer Science and Engineering*, pages 1253–1264. J. Wiley and Sons, Englewood Cliffs, 2009. Available from: http://dx.doi.org/10.1002/9780470050118.ecse159, doi:10.1002/9780470050118.ecse159.

[24] É. Chamberland, A. Fortin, and N. Tardieu. Solutions analytiques de problèmes de contact en grandes déformations. In *Neuvième colloque national en calcul des structures*, volume II, pages 671–676, Giens, France, 2009. Hermès. Available from: http://www.giref.ulaval.ca/~ericc/publications/mms_contact_uni_final.pdf.